Physical Modeling and Data Analysis of the Dynamic Response of a Flexibly Mounted Rotor Mechanical Seal

An Sung Lee
Korea Institute of Machinery and Metals,
Daejeon 305-600, Korea

Itzhak Green[1]
George W. Woodruff School
of Mechanical Engineering,
Georgia Institute of Technology,
Atlanta, GA 30332-0405

The dynamic behavior of mechanical face seals has been an active area of research over the past three decades. Analytical and experimental investigations have exclusively been devoted to the flexibly mounted stator (FMS) seal. Recent theoretical work on the dynamics of the noncontacting flexibly mounted rotor (FMR) seal has proven that it excels in every aspect of dynamic behavior compared to the FMS seal. The advantages of the FMR seal, however, have to be experimentally verified. This work introduces a physical model (i.e., test rig) for an experimental investigation of the dynamic behavior of a noncontacting FMR seal. Features of the test rig, a new method of modeling and measuring the stiffness and damping of elastomeric O-ring secondary seals, and data analysis procedures will be introduced. Finally, experimental results will be compared with theory.

Introduction

Conventional contacting seals are load unbalanced. The unbalanced load forces the seal faces into mechanical contact. Since wear increases with speeds, pressures, and temperatures common in high performance turbomachinery, noncontacting mode of operation is mandated. In noncontacting seals a thin fluid film lubricates the seal faces, which reduces friction losses and wear. A major consideration in engineering long-lasting noncontacting operation with minimum leakage is seal dynamics (see reviews by Etsion, 1982, 1985, and 1991 and Allaire, 1984).

Experimental work pertinent to seal dynamics is briefly reviewed in the following: Etsion and Burton (1979) tested a face seal model that consisted of a rigidly mounted rotor and a flexibly mounted stator under eccentric loading, i.e., initial stator misalignment. Self-excited oscillations in the form of combined precession and nutation of the stator were observed. Metcalfe (1982) analyzed the dynamic tracking ability of a flexibly mounted face to an angular misalignment of a fixed face, and experimentally observed the dynamic whirl to be close to half of the shaft speed in a well-aligned mechanical face seal. Sehnal et al. (1983) experimentally investigated the effects of face coning on the seal performance by comparing torque, face temperature, leakage, and wear of a conventional flat-face seal with three coned face seals. Etsion and Constantinescu (1984) experimentally observed the dynamic behavior of a noncontacting flexibly mounted stator (FMS) mechanical face seal. They showed that the stator misalignment and its phase shift are time dependent. With regard to commonly used elastomeric O-ring secondary seals Green and Etsion (1986) experimentally measured their stiffness and damping coefficients using a frequency excitation method.

Theoretical work on the dynamics of a noncontacting flexibly mounted rotor (FMR) mechanical face seal has recently been performed by Green (1987, 1989, and 1990). These showed that the FMR seal is inherently stable independent of operating speed if the transverse moment of inertia over the polar moment of inertia, I_t/I_p, is less than one (a ratio practical in commonplace mechanical face seals). Further, the FMR seal was found to be better configuration than the FMS seal in terms of various seal performance criteria, i.e., the total relative misalignment, critical stator misalignment, and threshold speed of instability in the case where the inertia ratio is greater than one. However, no experimental investigation of the dynamic behavior of a noncontacting FMR seal has ever been reported. Such an investigation is essential to corroborate the theoretical results and the advantages of the FMR seal. This work undertakes this task. Features of a dedicated test rig, a new method of modeling and measuring the stiffness and damping of elastomeric O-ring secondary seals, and data analysis procedures will be introduced.

The equations of motion for a noncontacting FMR mechanical face seal were derived by Green (1990). The equations of motion in the angular mode are presented here in the inertial $\xi\eta\zeta$-system (see the Nomenclature for definitions)

[1]On leave until July 31, 1994, at: Technion-Israel Institute of Technology, Faculty of Mechanical Engineering, Haifa 32000, Israel.

Contributed by the Tribology Division of THE AMERICAN SOCIETY OF MECHANICAL ENGINEERS and presented at the ASME/STLE Tribology Conference, Maui, Hawaii, October 16-19, 1994. Manuscript received by the Tribology Division February 24, 1994; revised manuscript received June 28, 1994. Paper No. 94-Trib-21. Associate Technical Editor: R. F. Salant.

$$I_t\ddot{\gamma}_\xi + I_p\omega\dot{\gamma}_\eta + (D_s+D_f)\dot{\gamma}_\xi + \left(D_s+\frac{1}{2}D_f\right)\omega\gamma_\eta + (K_s+K_f)\gamma_\xi$$
$$= \gamma_s\left(K_f\cos\psi_s + \frac{1}{2}D_f\omega\sin\psi_s\right) + K_s\gamma_{ri}\cos\omega t$$
$$I_t\ddot{\gamma}_\eta - I_p\omega\dot{\gamma}_\xi + (D_s+D_f)\dot{\gamma}_\eta - \left(D_s+\frac{1}{2}D_f\right)\omega\gamma_\xi + (K_s+K_f)\gamma_\eta$$
$$= \gamma_s\left(K_f\sin\psi_s - \frac{1}{2}D_f\omega\cos\psi_s\right) + K_s\gamma_{ri}\sin\omega t \quad (1)$$

The fixed stator misalignment, γ_s, and the initial rotor misalignment, γ_{ri}, are defined with respect to the axis of shaft rotation, and are always present due to manufacturing and assembly tolerances. These misalignments act as forcing inputs upon the rotor. A closed-form solution for the steady-state response of Eq. (1) was obtained in terms of transmissibilities by Green (1989) as follows:

$$\frac{\gamma_{rs}}{\gamma_s} = \frac{\sqrt{K_f^2+\frac{1}{4}D_f^2\omega^2}}{\sqrt{K^2+(D_s\omega+\frac{1}{2}D_f\omega)^2}}$$

$$\frac{\gamma_{rI}}{\gamma_{ri}} = \frac{K_s}{\sqrt{\left[(I_p-I_t)\omega^2+(K_s+K_f)\right]^2+\left(\frac{1}{2}D_f\omega\right)^2}} \quad (2)$$

where γ_{rs} and γ_{rI} are the rotor responses to γ_s and γ_{ri}, respectively. These theoretical transmissibilities are the subject of the investigation and they will be compared with the experimental ones.

Test Rig

The schematic of the noncontacting FMR mechanical face seal test rig is shown in Fig. 1. Instrumentation and rig assembly are shown photographically in Fig. 2. The faces of the stator and the carbon graphite ring, that was attached to the rotor, form the sealing dam. Separation of the faces was achieved by utilizing the hydrostatic effect, i.e., water pressure that drops in a converging gap between the flat-face carbon graphite ring and the coned-face stator. To allow rotor tracking to stator misalignment the rotor was flexibly mounted onto the shaft through an elastomeric O-ring foundation and a spring (details are given later).

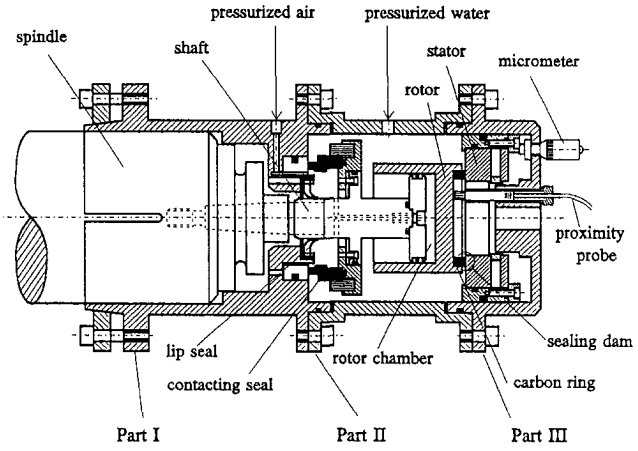

Fig. 1 Schematic of a noncontacting FMR seal test rig

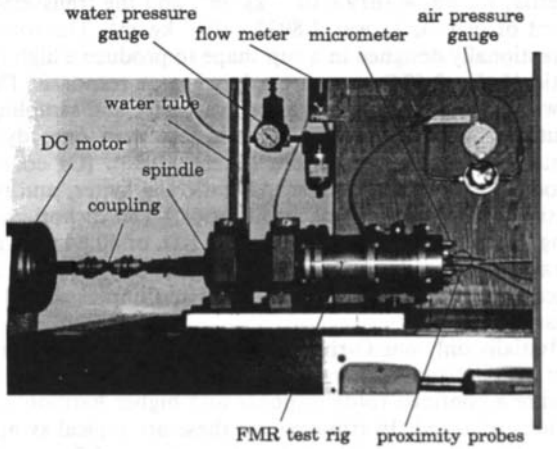

Fig. 2 Photograph of the rig assembly and instrumentation

Air pressure, which was supplied through holes in the shaft into the rotor chamber, regulated the seal clearances at the sealing dam. The pressurized air and pressurized water were separated by a contacting mechanical seal at one end, and the pressurized air was sealed by a lip seal at the other end. The shaft was screwed into a precision spindle which was driven by a motor mounted on a separate structure through a wafer spring coupling. For convenience of manufacturing, maintenance, and adjusting of the rig, the housing was made of three parts. All possible leakage paths were sealed by O-rings. The stator misalignment was adjusted by three micrometers, and the position of the rotor was detected by three eddy current proximity probes whose signals were sampled by a data ac-

Nomenclature

C = seal clearance
d_r = total displacement of rotor
d_{rI} = displacement of rotor due to γ_{ri}
d_{rs} = displacement of rotor due to γ_s
D = $D_f + D_s$
D_f = fluid film damping
D_s = support damping
I_p = polar moment of inertia
I_t = transverse moment of inertia
k_{rel} = relaxation stiffness, Eq. (3)
K_0, K_1 = viscoelastic stiffness constants, Eq. (3)
K = $K_f + K_s$
K_f = fluid film stiffness
K_s = support stiffness
p_w = water pressure
Q^* = leakage, Eq. (24)
Q = dimensionless leakage
r_i = inner radius
r_o = outer radius
R_i = dimensionless inner radius, r_i/r_o
R_m = dimensionless mean radius, $(1+R_i)/2$
t = time
α = viscoelastic decay constant, Eq. (3)
β^* = coning
β = dimensionless coning, $\beta^* r_o/C$
γ_r = total rotor response
γ_{ri} = initial rotor misalignment
γ_{rI} = rotor response due to γ_{ri}
γ_s = fixed stator misalignment
γ_{rs} = rotor response due to γ_s
ξ, η, ζ = inertial coordinate systems, Fig. 8
γ_ξ, γ_η = rotor misalignment in the $\xi\eta\zeta$-system
μ = viscosity
ψ_s = phase (shift) angle of γ_s
ω = shaft angular velocity

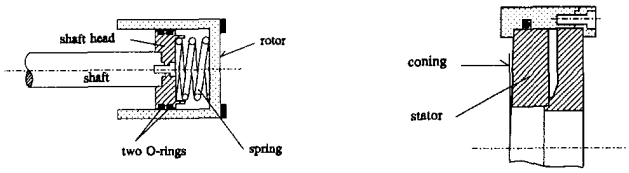

(a) Shaft head design (b) Coning mechanism of the stator

Fig. 3 Rotor and stator design

quisition board operated by personal computer. Leakage was measured by a flow meter placed on the supply line of the pressurized water. To assure that the measured response is that of the rotor, the shaft was made short and stiff [see Lee and Green (1994a)].

Rotor (Primary Ring) and Support System. The 0.5198 kg rotor was made of AISI 4140 Steel. The polar moment of inertia, I_p, was 4.1619×10^{-4} kg·m^2, and the transverse moment of inertia, I_t, was 2.8032×10^{-4} kg·m^2. The rotor was intentionally designed in a cup shape to produce a high inertia ratio ($I_t/I_p=0.674$) to secure a large rotor response. This allowed for the highest measuring sensitivity and sampling resolution. Since this inertia ratio is less than one, dynamic instability was not a concern (Green, 1990). (Of course, in production seals the smaller that ratio the better, and typical designs inherently possess small ratios.) The carbon graphite ring had an O.D. of 50.8 mm and an I.D. of 40.64 mm, giving a radius ratio, $r_i/r_o=0.8$. The rotor geometry rendered a balance ratio of 0.5 assuming flat faces and unpressurized rotor chamber.

Initially only one O-ring secondary seal was used. Series of test runs indicated that one O-ring support was insufficient to ensure a confined rotor response and higher harmonic oscillations occurred. In tribosystems these are typical symptoms of malfunction and failure is imminent. Lee and Green (1994b) analyzed this phenomenon and identified rubbing contact between the rotor and stator as the source of the oscillations. A shaft head having the support system of two Nitrile (Buna-N) O-rings and one spring was subsequently constructed [Fig. 3(*a*)]. The rotor response was dramatically improved and the higher harmonic oscillations were eliminated.

Stator (Mating Ring). The stator was made of 440 C stainless steel. Its face was heat-treated and hardened to 62 Rockwell C to reduce damage due to abrasive wear. The face was then polished to the flatness of two Helium light bands. Coning, which is important for axial and angular stiffnesses of the fluid film, was induced into the stator face by the mechanism shown in Fig. 3(*b*). By adjusting the tightening torque of the circumferentially distributed bolts the stator deformed, and various coning angles could be obtained.

Data Acquisition. Voltage signals from the proximity probes went through a low-pass filter and amplifier (cut-off frequency of 1000 Hz) useful in eliminating high frequency cross-talk noises among the probes. A potentiometer then dropped the amplified signal to the voltage specification of a data acquisition board capable of 100 kHz maximum sampling rate. The board was driven by a personal computer with real time data acquisition software.

Relaxation Test of O-Rings

To perform a dynamic analysis of a seal the dynamic properties of the flexible support [K_s and D_s in Eq. (2)] must be known. To obtain the stiffness and damping coefficients of the O-rings, a test similar to that in Green and Etsion (1986) would be necessary. Such an experiment is rather involved in instrumentation and analysis, and is a significant undertaking by itself. Instead, a much simpler procedure is developed here

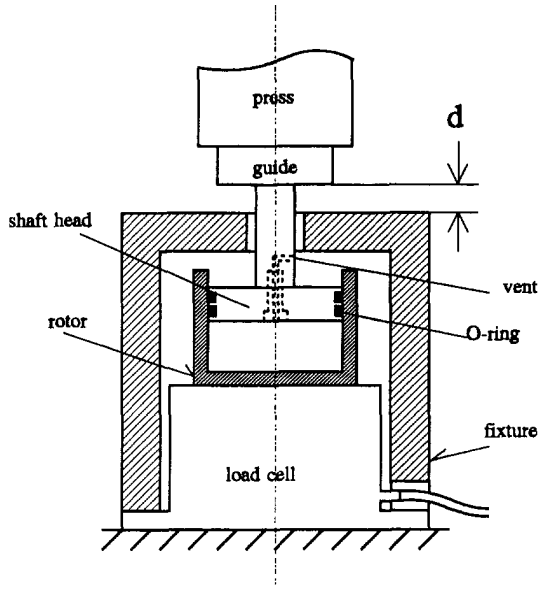

Fig. 4 Schematic of O-ring relaxation test rig

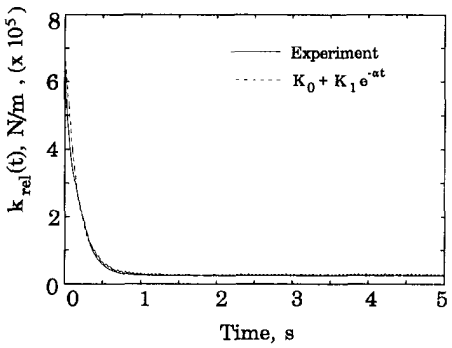

Fig. 5 Measurement of O-Ring relaxation stiffness

based on the work by Szumski and Green (1991). In this procedure the dynamic coefficients are calculated in the frequency domain from relaxation data obtained in the time domain. The advantage of a relaxation test is that it is simple and that it can be directly performed on the mechanical parts of the actual seal test rig.

The schematic of a test apparatus to measure the axial relaxation force of the two Buna-N O-rings is shown in Fig. 4. The O-rings (hardness 70 Shore A) had an inner diameter of 37.69 mm and a cross section wire diameter of 3.53 mm. The O-rings were installed unlubricated in the shaft head grooves, with five percent stretch and seven percent squeeze. The guide was rapidly driven down by the press, a small step displacement, d, of 75 microns average. That instantaneous displacement induced a resisting force that was measured by a load cell. The force in the O-rings relaxed in time characteristically of elastomeric materials. The relaxation force was then divided by the step displacement to give a relaxation stiffness, $k_{rel}(t)$, the average of which is shown as a solid line in Fig. 5. Tests were performed at room temperature and ambient pressure. [Smaller values of d were tried giving largely repeatable results; however, a relatively large value of 75 microns was preferred because it produced the highest load cell response (i.e., resolution) without causing O-ring slip.]

A comprehensive discussion of viscoelastic constitutive (stress-strain) equations is given in Szumski and Green (1991). Consolidation of O-ring geometry and boundary conditions with these yields effective stiffness (force-displacement) equations. The simplest representation of the time domain stiffness, $k_{rel}(t)$, is through a degenerated Prony series

$$k_{rel}(t) = K_0 + K_1 e^{-\alpha t} \tag{3}$$

The parameters K_0, K_1, and α can be obtained by fitting Eq. (3) to the data in Fig. 5. At zero time $k_{rel}(0)$ is the glassy stiffness, and after long times $k_{rel}(\infty)$ is the rubbery (fully relaxed) stiffness. These two were extracted from the data in Fig. 5. From Eq. (3) we have

$$K_0 + K_1 = k_{rel}(0)$$
$$K_0 = k_{rel}(\infty)$$
$$\alpha = \frac{K_1}{\int_0^\infty [k_{rel}(t) - K_0]dt} \tag{4}$$

First K_0 and K_1 are determined and then the decay parameter, α, is calculated using numerical integration, where $k_{rel}(t)$ is taken from the experimental data points. This procedure resulted in $K_0 = 2.31 \times 10^4$ N/m, $K_1 = 6.88 \times 10^5$ N/m, and $\alpha = 6.03$ s^{-1}. The calculated $k_{rel}(t)$, with these parameters substituted in Eq. (3), demonstrates an excellent fit in Fig. 5.

The force-displacement constitutive relationship for a viscoelastic material can be expressed in analogy to the stress-strain constitutive relationship (see Szumski and Green, 1991)

$$f(t) = \frac{d}{dt}\int_0^t k_{rel}(\tau)u(t-\tau)d\tau = \frac{d}{dt}\int_0^t k_{rel}(t-\tau)u(\tau)d\tau \tag{5}$$

where $f(t)$ is a time dependent force caused by a displacement time history, $u(t)$. Taking the Laplace Transform of Eq. (5) gives

$$F(s) = sK_{rel}(s)U(s) \tag{6}$$

where s is the Laplace parameter. A complex impedance, $Z(s)$, emerges

$$Z(s) = sK_{rel}(s) \tag{7}$$

Hence, taking the Laplace Transform of the postulated constitutive Eq. (3) and multiplying by s gives

$$Z(s) = K_0 + \frac{K_1 s}{s+\alpha} \tag{8}$$

Now assuming harmonic excitation, the frequency dependent complex impedance, $Z(j\omega)$, is obtained by replacing s with $j\omega$ in Eq. (8):

$$Z(j\omega) = K_0 + \frac{K_1\omega^2}{\alpha^2+\omega^2} + j\frac{K_1\alpha}{\alpha^2+\omega^2}\omega \tag{9}$$

Finally, the frequency dependent stiffness and damping, $K_{axial}(\omega)$ and $D_{axial}(\omega)$, are obtained from the real and imaginary parts of $Z(j\omega)$, respectively,

$$K_{axial}(\omega) = \mathrm{Re}[Z(j\omega)] = 2.31 \times 10^4 + \frac{6.88 \times 10^5 \omega^2}{36.36+\omega^2} \quad [\mathrm{N/m}] \tag{10}$$

$$D_{axial}(\omega) = \frac{Im[Z(j\omega)]}{\omega} = \frac{4.15 \times 10^6}{36.36+\omega^2} \quad [\mathrm{N \cdot s/m}] \tag{11}$$

where K_0, K_1, and α have been substituted, and ω is taken in rad/s. Since a relaxation test was performed along the shaft axis the subscript axial was added to the parameters.

As described above, Eqs. (10) and (11) were obtained from a constitutive relationship of Eq. (3). [More elaborate constitutive equations (Szumski and Green, 1991) will produce different Eqs. (10) and (11).] In contrast, the stiffness and damping of O-rings measured by Green and Etsion (1986) were postulated to behave empirically in the frequency domain according to $K_{axial} = A\omega^B$, and $D_{axial} = a\omega^b$. A deficiency of the latter is that it predicts unrealistsic zero static stiffness, and unbounded stiffness at very high frequencies. Equation (10) does not have these deficiencies. Furthermore, Eqs. (10) and (11) were obtained from data of a test that was performed on the actual O-rings, rotor, and shaft head, i.e., parts of the seal test rig itself.

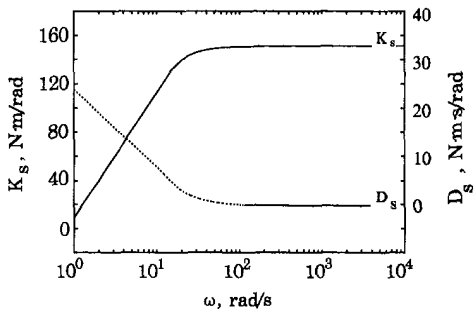

Fig. 6 Support angular stiffness and damping as a function of shaft speed

Once the axial dynamic properties of the O-rings are known, their equivalent angular values can be obtained from (see Appendix in Green and Etison, 1985):

$$K_s \equiv K_{angular} = \frac{1}{2} r^2 K_{axial} \tag{12}$$

$$D_s \equiv D_{angular} = \frac{1}{2} r^2 D_{axial} \tag{13}$$

where r is the mean radius of the O-ring (here $r = 20.61$ mm). In the test rig the support included a compression spring. Equation (12) was also used to find the equivalent angular stiffness of the spring whose axial stiffness was 2070 N/m. Ultimately for the entire support (O-rings and spring), the angular stiffness and damping, K_s and D_s, were found to be

$$K_s = 5.346 + \frac{146.1\omega^2}{36.36+\omega^2} \quad [\mathrm{N \cdot m/rad}] \tag{14}$$

$$D_s = \frac{881.4}{36.36+\omega^2} \quad [\mathrm{N \cdot m \cdot s/rad}] \tag{15}$$

The plots of K_s and D_s as a function of ω are shown in Fig. 6. A transition from rubbery to glassy occurs between 1 to 100 rad/s, where K_s increases and D_s decreases to constant values.

Data Analysis

Reference Plane and Misalignments. A rotor reference plane perpendicular to the shaft axis had to be defined to measure the rotor misalignment. Operation of the rig without the stator and water showed that the rotor responses were sinusoidal and synchronous with the shaft speed (Fig. 7). The mean values of the rotor responses defined the rotor reference plane. Then, the initial rotor misalignment, γ_{ri}, was measured by the probes with respect to the rotor reference plane under the same conditions, except that the shaft was stationary at that time. The fixed stator misalignment, γ_s, was measured with respect to the rotor reference plane by the following procedure: First, the stator was replaced in the test rig. Then, full contact between the rotor and stator was imposed by pressurizing the rotor chamber. At that state the rotor misalignment, as measured by the probes, assumed the misalignment of the stator, γ_s.

Calculation of Misalignment and Precession. With reference to Fig. 8 and vector algebra the misalignment and precession of the rotor could be found. ξ and ζ are inertial reference axes where the latter coincides with the axis of shaft rotation. A, B, and C are points in the rotor plane as measured by the three probes. A unit normal vector out of the plane, **n**, is defined by

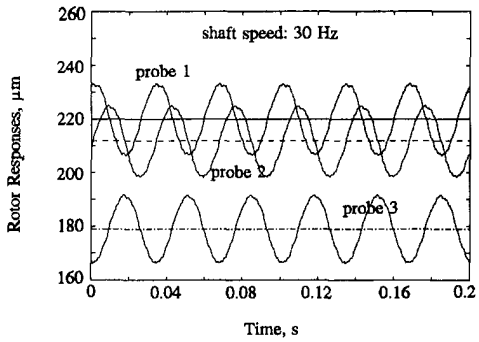

Fig. 7 Rotor responses without the stator and water

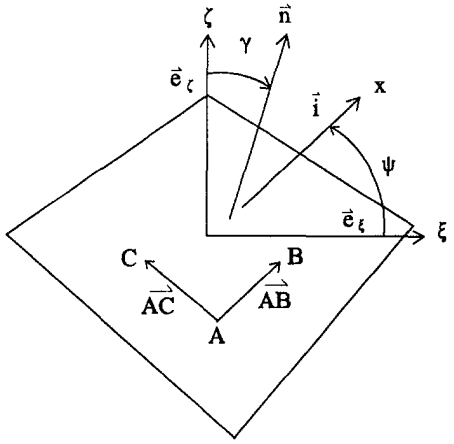

Fig. 8 Misalignment and precession of a plane

$$\mathbf{n}=\frac{\mathbf{AB}\times\mathbf{AC}}{|\mathbf{AB}\times\mathbf{AC}|} \tag{16}$$

and, therefore, the misalignment (nutation) of the plane, γ, is obtained by

$$\mathbf{e}_\zeta\cdot\mathbf{n}=\cos\gamma;\quad \therefore\gamma=\cos^{-1}(\mathbf{e}_\zeta\cdot\mathbf{n}) \tag{17}$$

The axis about which the nutation occurs, x, is defined by its unit vector

$$\mathbf{i}=\frac{\mathbf{e}_\zeta\times\mathbf{n}}{|\mathbf{e}_\zeta\times\mathbf{n}|} \tag{18}$$

and the precession angle, ψ, between ξ and x, is obtained by

$$\mathbf{e}_\xi\cdot\mathbf{i}=\cos\psi;\quad \therefore\psi=\cos^{-1}(\mathbf{e}_\xi\cdot\mathbf{i}) \tag{19}$$

Separation of Total Rotor Misalignment Into Components. The total rotor misalignment vector, γ_r, is the superposition of two components (Green, 1989)

$$\boldsymbol{\gamma}_r=\boldsymbol{\gamma}_{rs}+\boldsymbol{\gamma}_{rI} \tag{20}$$

To compare the experimental rotor responses with the theoretical transmissibilities of Eq. (2), the separation of $\boldsymbol{\gamma}_r$ into its components, $\boldsymbol{\gamma}_{rs}$ and $\boldsymbol{\gamma}_{rI}$, is necessary. A model of the rotor response, γ_{rs}, caused by the stator misalignment, γ_s (while assuming the absence of γ_{ri}), is illustrated in Fig. 9(*a*). Since γ_s is a constant magnitude space-fixed angle, γ_{rs} is also of the same nature, i.e., a constant magnitude space-fixed angle. A model of the rotor response, γ_{rI}, caused by its own initial (static) misalignment, γ_{ri} (while assuming the absence of γ_s), is illustrated in Fig. 9(*b*). Since γ_{ri} is rotating at a shaft speed and is of constant magnitude, γ_{rI} is also of the same nature, i.e., rotating at the shaft speed and of constant magnitude. This superposition is inherently imbedded in the probe readings. Hence, it is recognized that the total displacement of the rotor at any of the three probe locations, $d_{r,j}(j=1, 2, 3)$, is

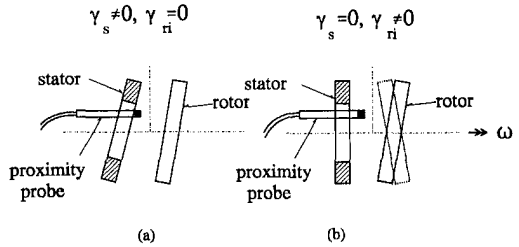

Fig. 9 Models of rotor responses to the misalignments

the sum of a constant displacements $d_{rs,j}$ caused by γ_s, and an oscillating displacement $d_{rI,j}$ caused by γ_{ri}:

$$d_{r,j}=d_{rs,j}+d_{rI,j}=d_{rs,j}+|d_{rI}|\cos(\omega t-\phi_j),\quad j=1, 2, 3 \tag{21}$$

where ϕ_j is a phase angle. The mean values of $d_{r,j}$ are

$$d_{rs,j}=\frac{1}{N}\sum_{k=1}^{N}d_{r,jk},\quad j=1, 2, 3 \tag{22}$$

where N is the number of data points in one shaft revolution. The subtracted values of $d_{r,j}$ by $d_{rs,j}$ are

$$d_{rI,j}=d_{r,j}-d_{rs,j},\quad j=1, 2, 3 \tag{23}$$

Now, γ_{rs}, γ_{rI}, and their corresponding precessions can be calculated from $d_{rs,j}$ and $d_{rI,j}$, respectively, using the coordinates of the probes (radial position 12.7 mm) and Eqs. (16)–(19).

Seal Clearance. Since the fluid film stiffness and damping of the FMR seal depend upon the seal clearance, the dynamic behavior of the FMR seal will be affected by it. Thus, controlling the seal clearance at a prescribed value during experiment is important. Etsion and Constantinescu (1984) used a simplified leakage equation to calculate the seal clearances of the noncontacting FMS seal. That equation is valid for the FMR seal as well. Hence,

$$Q^*=\frac{\pi p_w}{6\mu}C^3Q;\quad Q=\frac{R_m}{1-R_i}\left[1+\frac{3}{2}\beta(1-R_i)\right] \tag{24}$$

where Q^* is the leakage, p_w is the sealed water pressure, C is the seal clearance, and Q is the dimensionless leakage. Even if a relatively large error is present in the value of Q, the error will much less affect the value of C because a cubic root is taken according to Eq. (24). This extraction provides the best estimate of the seal clearance since it is based on the actual (measured) flow rate in the rig.

Test Procedure and Results

Operation of the test rig was performed at a reference water pressure of 0.2068 MPa, and a coning angle of 0.0112 rad. The shaft speeds was varied from 600 to 1800 rpm in increments of 300 rpm. The leakage was monitored by the flow meter, and kept at 0.833×10^{-6} m^3/s by controlling air pressure in the rotor chamber. The seal clearance was found to be 3.75 microns by using Eq. (24). The misalignment inputs, γ_s and γ_{ri}, were found to be 7.19×10^{-4} rad and 5.22×10^{-4} rad, respectively.

A typical time response of the rotor, $d_{rI,j}$, at one probe position due to γ_{ri} is shown in Fig. 10. $d_{rI,j}$ was obtained after subtracting the mean value, $d_{rs,j}$, from $d_{r,j}$. Its power spectral density had a big spike at the shaft speed of 30 Hz (1800 rpm), and negligible values at higher frequencies (Lee and Green, 1994). The corresponding trajectory of the rotor misalignment vector, γ_{rI}, as a function of time, is shown in Fig. 11. It was obtained after filtering out the high frequency components. In Fig. 11, the distance from the origin to a point on the trajectory is the angular response magnitude, and the angle between the line connecting the origin to the point and the ξ-axis is the precession. The order of γ_{rI} was 10^{-4} rad and this

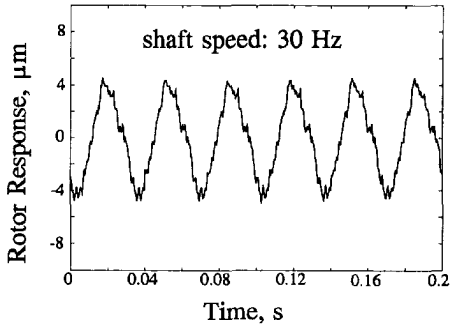

Fig. 10 Typical rotor response to the initial rotor misalignment at one probe location

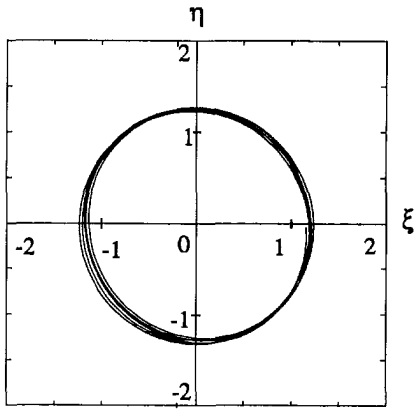

Fig. 11 Trajectory of the rotor misalignment vector (units of ξ and η are 0.1 mrad)

justifies the treatment of γ_{rI} as a vector. From Figs. 10 and 11, respectively, it can be noticed that the experimentally obtained γ_{rI} had the same frequency as the shaft speed and its magnitude was constant. This is precisely what the theory by Green (1989) predicted. The experimental static (γ_{rs}/γ_s) and dynamic (γ_{rI}/γ_{ri}) transmissibilities at various shaft speeds are summarized in Table 1, along with the theoretical counterparts. A comparison between experimental and theoretical values reveals a maximum deviation of 15 percent, overall indicating very good agreement.

Conclusions

To experimentally investigate the dynamic behavior of a noncontacting FMR mechanical face seal, a test rig was designed and built. Features of the rig design and methods required to analyze experimental data were introduced. Precautions were taken to ensure that measured response is that of the flexibly mounted rotor.

A new approach to modeling and measuring the stiffness and damping of elastomeric O-ring secondary seals was introduced. This was based on fundamental theory and a realistic constitutive equation. Representation can easily be moved from the time domain to the frequency domain. The time domain information was extracted from a relaxation test, a far simpler procedure than customary frequency excitation tests. The resulting stiffness and damping are realistic having rubbery, transition, and glassy properties.

Measurements from the rig and data analysis indicated that the qualitative and quantitative behavior of the FMR seal agreed very well with theoretical predictions. Since a "half frequency whirl" (Green, 1990) was not present in the test results, it

Table 1 Experimental and theoretical transmissibilities at $p_w = 0.2068$ MPa and $C = 3.75$ μm

Shaft speed (rpm)	γ_{rs}/γ_s		γ_{rI}/γ_{ri}	
	Exp.	Theo.	Exp.	Theo.
600	0.6916	0.7602	0.2762	0.2392
900	0.6769	0.7595	0.2323	0.2398
1200	0.7013	0.7593	0.2459	0.2397
1500	0.7519	0.7593	0.2340	0.2394
1800	0.6676	0.7594	0.2442	0.2388

verified that dynamic instability was not a problem (this is because the rotor had an inertia ratio, I_t/I_p, less than one). The measured rotor response, γ_{rI}, had the shaft frequency and its magnitude was constant as predicted by the theory (Green, 1989). At this stage the physical model and data analysis have proven viable for further exhaustive testing under variations of operating conditions, i.e., a parametric experimental investigation.

Acknowledgment

This work was supported in part by the National Science Foundation under Grant Number MSM-8619190. This support is gratefully acknowledged. The authors would like to thank Mr. Ariel Trau (of the Israel Armament Development Authority) and Dr. Scott Bair (of Georgia Tech) who helped in the design and construction of a prototype test rig.

References

Allaire, P. E., 1984, "Noncontacting Face Seals for Nuclear Applications—A Literature Review," *Lubrication Engineering*, Vol. 40, 6, pp. 344-351.

Etsion, I., and Burton, R. A., 1979, "Observation of Self-Excited Wobble in Face Seals," ASME JOURNAL OF LUBRICATION TECHNOLOGY, Vol. 101, 4, pp. 526-528.

Etsion, I., 1982, "A Review of Mechanical Face Seal Dynamics," *The Shock and Vibration Digest*, Vol. 14, 4, pp. 9-14.

Etsion, I., 1985, "Mechanical Face Seal Dynamics Update," *The Shock and Vibration Digest*, Vol. 17, 4, pp. 11-15.

Etsion, I., 1991, "Mechanical Face Seal Dynamics 1985-1989," *The Shock and Vibration Digest*, Vol. 23, 4, pp. 3-7.

Etsion, I., and Constantinescu, I., 1984, "Experimental Observation of the Dynamic Behavior of Noncontacting Coned-Face Mechanical Seals," *ASLE Trans.*, Vol. 27, 3, pp. 263-270.

Green, I., and Etsion, I., 1985, "Stability Threshold and Steady-State Response of Noncontacting Coned-Face Seals," *ASLE Trans.*, Vol. 28, 4, pp. 449-460.

Green, I., and Etsion, I., 1986, "Pressure and Squeeze Effects on the Dynamic Characteristics of Elastomer O-Rings Under Small Reciprocating Motion," ASME JOURNAL OF TRIBOLOGY, Vol. 108, 3, pp. 439-445.

Green, I., 1987, "The Rotor Dynamic Coefficients of Coned-Face Mechanical Seals with Inward or Outward Flow," ASME JOURNAL OF TRIBOLOGY, Vol. 109, No. 1, pp. 129-135.

Green, I., 1989, "Gyroscopic and Support Effects on the Steady-State Response of a Noncontacting Flexibly Mounted Rotor Mechanical Face Seal," ASME JOURNAL OF TRIBOLOGY, Vol. 111, pp. 200-208.

Green, I., 1990, "Gyroscopic and Damping Effects on the Stability of a Noncontacting Flexibly-Mounted Rotor Mechanical Face Seal," *Dynamics of Rotating Machinery*, Hemisphere Publishing Company, pp. 153-173.

Lee, A. S., and Green, I., 1994a, "Rotordynamics of a Mechanical Face Seal Riding on a Flexible Shaft," ASME JOURNAL OF TRIBOLOGY, Vol. 116, 2, pp. 345-351.

Lee, A. S., and Green, I., 1994b, "Higher Harmonic Oscillations in a Noncontacting FMR Mechanical Face Seal Test Rig," ASME *Journal of Vibration and Acoustics*, Vol. 116, 2, pp. 161-167.

Metcalfe, R., 1982, "Dynamic Whirl in Well-Aligned, Liquid-Lubricated End-Face Seals with Hydrostatic Tilt Instability," *ASLE Trans.*, Vol. 25, 1, pp. 1-6.

Sehnal, J., et al., 1983, "Performance of the Coned-Face End Seal with Regard to Energy Conservation," *ASLE Trans.*, Vol. 26, 4, pp. 415-429.

Szumski, R., and Green, I., 1991, "Constitutive Laws in Time and Frequency Domains for Linear Viscoelastic Materials," Invited presentation at the Acoustical Society of America Conference, Houston TX, Paper No. 4SA1.